Examining the feedback signals used in closed-loop control of intense laser fragmentation of CO^+

E. Wells,* Michael Todt, Bethany Jochim, Neal Gregerson, R. Averin, Nathan G. Wells, N. L. Smolnisky, and Nathan Jastram
Department of Physics, Augustana College, Sioux Falls, South Dakota 57197, USA

J. McKenna, A. M. Sayler, Nora G. Johnson, M. Zohrabi, B. Gaire, K. D. Carnes, and I. Ben-Itzhak
J.R. Macdonald Laboratory, Department of Physics, Kansas State University, Manhattan, Kansas 66506, USA
(Received 5 September 2009; published 1 December 2009)

A closed-loop feedback system is used to determine the optimal pulse shapes for manipulating the branching ratio of carbon monoxide following ionization by an intense laser pulse. We focus on manipulating the $C^+ + O$ and $C + O^+$ branching ratios of excited states of transient CO^+. The feedback control system consists of a high resolution time-of-flight spectrometer coupled via a genetic feedback algorithm to an acousto-optical programmable dispersive filter that is incorporated into the ultrafast laser system. Using the spectrometer resolution to distinguish dissociation pathways and select a specific pathway to drive the algorithm, we are able to demonstrate enhanced control of some fragmentation channels. Principal control analysis indicates that the more specific feedback results in numerically simpler optimal pulse shapes. The combination of a more specific target and reduction in pulse complexity could lead to more straightforward investigations of the control mechanism. Analysis of the pulse shapes in conjunction with measurement of the fragment kinetic energy release distributions obtained from the optimized laser pulses is used to probe the dissociative ionization mechanisms.

DOI: 10.1103/PhysRevA.80.063402 PACS number(s): 32.80.Qk, 33.80.Rv, 42.50.Hz, 34.50.Gb

I. INTRODUCTION

Over the last decade, manipulation of atomic and molecular dynamics using shaped ultrafast laser pulses has become more common [1–13]. Due to the complexities of the interaction between the target atom or molecule and the intense laser field, it is difficult to make an *a priori* determination of the specific laser characteristics that will maximize the desired result. Furthermore, shaping methods using devices such as spatial light modulators [14] or acousto-optical modulators [15,16] allow for vast variation of the phase and amplitude parameters that constitute a pulse. A systematic search of the full parameter space is generally prohibitively difficult. Consequently, feedback algorithms [17–19] are often employed to arrive at the optimally controlling laser pulse. Genetic algorithms (GA) [20] are the most commonly used search optimization methods, although other techniques have been suggested (e.g., Ref. [21]). While these algorithms are powerful tools for searching a multidimensional phase space, they often produce complicated pulse shapes that yield only limited information about the control mechanism.

To further complicate this problem, the optimal fields are often not unique [9], and groups of solutions may form a continuous surface in the multidimensional phase space [22,23]. In addition, more sophisticated multiobjective algorithms are appearing [29,30], which can generate additional complexity in the pulse shapes. Gaining mechanistic insight, therefore, is difficult. There have been only a few reports of success at deconstructing the optimal laser pulse and thereby recovering information about the dynamics involved in the interaction [24–28]. If recent proposals to create quantum logic gates using tailored ultrafast laser pulses [31,32] are to be realized, however, a repeatable, robust approach to obtaining optimal pulse shapes will be needed. Developing these robust approaches will likely depend upon gaining a deeper understanding of the control mechanism(s).

In this article, we examine this problem within the framework of selective molecular fragmentation. A number of previous experiments have demonstrated closed-loop control of molecular fragmentation [2,3,5,9,10,13,24,33–41], typically using time-of-flight mass spectrometry (TOFMS) to obtain the feedback signal for the algorithm to maximize. As near as we can determine, in each of these cases, the feedback signal included an entire molecular ion species, identified by the mass to charge ratio (m/q) of the ion. This is understandable, especially when examining larger molecules, because in these cases the spectrometer must often be configured to detect a wide range of m/q. In the case of the C_{60} experiment [10], for example, the detected ions ranged from at least C_{60}^+ to C_{48}^{3+}, a range in m/q of 528.

On the other hand, it is known that even in the simplest case of H_2, dissociative ionization that includes a H^+ ion in the final state may occur from double-ionization, ionization-excitation [42], or ground-state dissociation [43]. Under the right conditions, TOFMS techniques can distinguish these channels [42,43], and there are examples of even higher resolution techniques [44]. Given this background, we investigate the following question: How is the control affected if only a subset of a particular m/q species is used as the feedback signal?

In our experiments, shaped intense laser pulses are used to control the fragmentation branching ratio of carbon monoxide. The selection of this target is something of a compromise: It is more complex than the previous H_2 example, and given the competition between dissociation pathways in the case of multiple ionization, it should offer a reasonable challenge for the GA. It is, however, still a fairly simple diatomic for which potential energy calculations exist for CO^+, CO^{2+},

*eric.wells@augie.edu

and CO^{3+} [45–49]. With an ionization potential of 14.014 eV, the optimal pulse will require substantial intensity to ionize and fragment the parent molecule. Carbon monoxide has also been a popular heteronuclear target for intense laser studies in the past (e.g., Refs. [50–56]), and we hope that insight gained from these previous studies may be applied to the interpretation of the shaped pulse results.

In this article, we report on how the degree to which the molecular fragmentation may be controlled depends on the exclusion of certain fragmentation channels from the feedback loop. Specifically, we alternate between the inclusion of C^+ and O^+ fragments from all possible transient CO^{q+} and selecting only fragments that originate from CO^+. The experimental setup is described in Sec. II. Section III includes the results and our analysis, including an examination of the relative pulse complexity for different feedback signals. Finally, we offer some explanation for how the inclusion of more fragmentation pathways influences the control mechanism.

II. EXPERIMENT

Our experimental setup consists of an ultrafast laser system with a pulse shaper, a high-resolution time-of-flight mass spectrometer, and a computer control that links them together and contains the genetic algorithm that uses the feedback signals to determine the optimal pulse shapes. The laser pulses are provided by a Ti:sapphire laser system based on chirped pulse amplification techniques. The output of the laser has a center wavelength of 790 nm, a pulse energy of 1 mJ, and a repetition rate of either 1 or 1.5 kHz. The bandwidth of the laser pulse is 30 nm, which results in a near Fourier transform-limited pulse duration of 35 fs full width at half maximum (FWHM). Transmission through the pulse shaper and the necessary beam transport optics lengthens the pulse somewhat. As a result, the shortest pulses available in the experiment are slightly longer.

The pulses are shaped with an acousto-optic programmable dispersive filter [57], commonly known as a "DAZZLER," which is manufactured by Fastlite [58]. The DAZZLER is located in the laser system after the oscillator and stretcher but before the amplifier. The DAZZLER can independently control the spectral amplitude and phase for a large number of spectral components. In practice we divide up the bandwidth into 16 regions and adjust only the phase in each of these regions. The phase is linearly interpolated between the centers of each of the regions by the DAZZLER software.

The laser is focused by a spherical mirror of focal length 75 mm to a point in the extraction region of a two-stage Wiley-McLaren [59] style time-of-flight (TOF) spectrometer. The laser focus is centered in the middle of the 12 mm extraction region, which has a field of 16.3 V/cm. The acceleration region is 10 mm long with a field of 127.6 V/cm, and the drift region is 555 mm and held at ground. The spectrometer is located in an ultrahigh vacuum chamber having a base pressure of about 5×10^{-10} Torr. The target CO gas was introduced into the chamber using a high precision leak valve so that the pressure could be controlled down to 1 $\times10^{-9}$ Torr. Typical target pressures for the experiment were in the 10^{-8} or 10^{-7} Torr range. The target CO gas has the same m/q as N_2, but the difference between the background and experiment pressures minimized the contribution from residual N_2 in the chamber. The lack of N^{2+} observed at laser intensities that produce significant C^{2+} and O^{2+} fragments verified that N_2 was not a significant source of ions in these experiments. While the laser could produce 1.0 mJ/pulse, in these experiments the maximum pulse energy was usually restricted to around 0.1 mJ/pulse. This translates to a peak intensity of about 1×10^{15} W/cm^2 for a transform-limited pulse. The beam waist is ~8 μm. The laser is linearly polarized with the polarization axis along the TOF axis in most cases. An aperture with a solid angle of 2.2×10^{-4} sr limited collection of molecular fragments to those predominately breaking along the TOF axis. Specific conditions for particular measurements are listed in Table I.

TABLE I. Summary of experimental results using different fitness targets from the strong-field dissociative ionization of CO. The "wide" and "narrow" designations refer to the inclusiveness of the gate settings as shown in Fig. 1. The final column shows the ratio of the fitness obtained with the optimal pulse to the fitness obtained with a transform-limited pulse with the same pulse energy.

Fitness target	Pulse energy (mJ)	Gate	$\frac{\text{Optimal}}{\text{TL}}$
$\frac{C^+}{O^+}$	0.065	Wide	1.40
$\frac{C^+}{O^+}$	0.115	Wide	1.17
$\frac{C^+ + O}{C + O^+}$	0.100	Narrow	1.08
$\frac{O^+}{C^+}$	0.065	Wide	1.25
$\frac{O^+}{C^+}$	0.120	Wide	1.20
$\frac{C + O^+}{C^+ + O}$	0.100	Narrow	1.94
$\frac{C^{2+}}{C^+}$	0.080	Wide	2.13
$\frac{C^+}{C^{2+}}$	0.080	Wide	8.23

Ions were detected by a microchannel plate (MCP) detector with the signals processed by one of two methods. In the conventional current mode detection, the analog current was measured as a function of time relative to a laser initiated photodiode signal. Gated integrators and boxcar averagers (Standford Research Systems Model SR250) were used to record the current from the regions of interest. The time constant of the integration was set at 1000 laser shots, and we recorded data for about 5000 shots for each trial pulse. These signals are sent to the control computer for use by the GA. The entire time-of-flight spectrum is monitored during the experiment and recorded using a digital oscilloscope. At the end of an experiment, we typically lowered the pressure in the chamber and switched to collecting data in pulse counting mode, using a constant fraction discriminator and a multihit time-to-digital converter. This allowed us to obtain higher-statistics time-of-flight spectra for detailed examination.

Our GA was fairly standard for this type of application and was based upon a freely available GA library [60]. Using the experimental results as feedback, we employ the GA to search for a set of laser pulses that best achieve some defined

target associated with the measured fragmentation branching ratio. The search algorithm specifies a "genetic code" for each laser pulse, or "individual." In our case, the genetic code consists of the phase delay in each of the 16 spectral regions discussed above. These values become the 16 genes on the chromosome that identifies our individual pulses. To begin the search, a "generation" of 50 or so individuals are created from random genetic sequences. The fitness of each individual in the generation is assessed according to its performance in achieving the specified target goal. In these experiments, the target goal is a ratio of different fragmentation channels of the transient CO^+, such as $[C^+ + O]/[C + O^+]$. To protect against division by zero in the case of no signal, we add an offset to the denominator of these ratios that is about 10% of the size of the denominator signal when a transform-limited pulse is present.

Individual pulses are selected to "mate" based upon a tournament selection operator. Individuals with higher fitness have a greater chance of being selected for reproduction. Subsequent generations of pulses are constructed by mating the identified parents using a two-point crossover operator in conjunction with a 2% probability of mutation per gene. These two operators define the genetic code of the offspring. We also use the elitism operator to add a genetic copy of the fittest individual into the next generation. The fitness of the individuals in the subsequent generation is then assessed using TOFMS, and the process is repeated until the GA converges on a solution. To check for experimental stability, we record the fitness for a transform-limited pulse between each generation.

III. RESULTS AND DISCUSSION

A summary of the separate experimental results obtained for the dissociative ionization of CO^{q+} are listed in Table I. Control over the branching ratios between different charge states was fairly easy to achieve, as indicated by the results of the $[C^{2+}]/[C^+]$ and $[C^+]/[C^{2+}]$ experiments. This is likely because the GA is simply modulating the intensity by stretching or narrowing the pulse duration. This, in turn, affects the amount of ionization as C^+ and C^{2+} come from different levels of ionization. It is more interesting to consider fitness targets that select between different outcomes involving fragments of the same intermediate charge state.

How does selecting a more specific final state for use as a feedback signal affect the control process? This topic was investigated with attempts to control the relative magnitude of C^+ and O^+ fragments. These fragment ions can originate from several sources, including CO^+ parent ions ($CO^+ \rightarrow C^+ + O$ or $CO^+ \rightarrow C + O^+$) and CO^{2+} parent ions ($CO^+ \rightarrow C^+ + O^+$). Asymmetric dissociation of higher charge states of the CO^{q+} is less likely and is not a major contribution in these experiments. With the laser polarization pointed along the TOF axis, these channels separate, as shown in Fig. 1. Fragment ions with higher kinetic-energy release (KER) are shifted forward and backward in time compared to lower energy fragment ions. Peak identities were verified by comparison to ion optics simulations [61] at various spectrometer voltages.

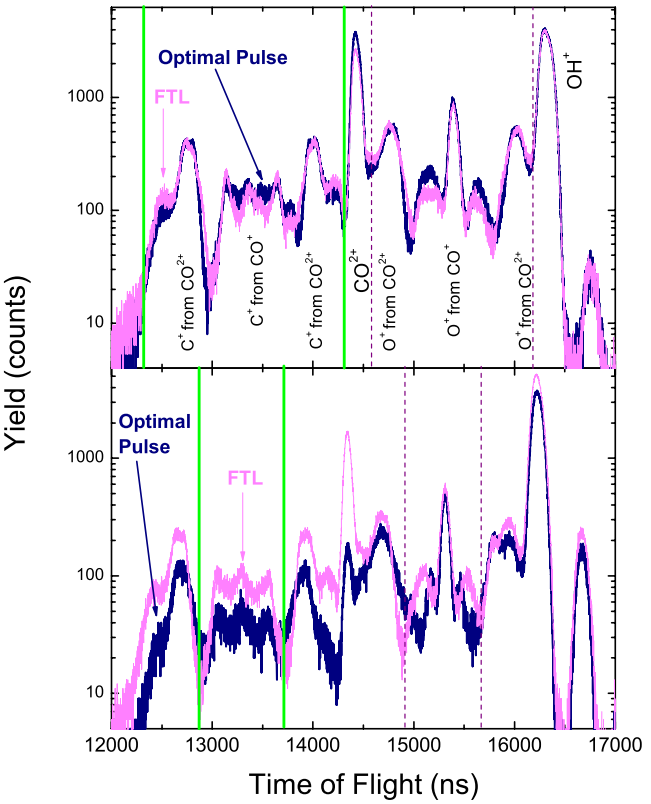

FIG. 1. (Color online) Time-of-flight spectra of the strong-field dissociative ionization of CO. Yields are normalized to the number of laser shots. (Top) spectra for the Fourier transform-limited pulse (denoted by the magenta line and labeled as FTL). The nearly overlapping thick blue line shows the spectra obtained with the GA determined optimal pulse for the O^+/C^+ fitness target with wide gate settings, represented by the solid green and dashed purple lines surrounding the C^+ and O^+ fragments. The pulse energy was 0.115 mJ/pulse in both cases. (Bottom) similar spectra, but with narrow gates on the GA run. The pulse energy was 0.100 mJ/pulse.

By judicious gating on the TOF spectra, we can experimentally select between integrating all ions of a particular m/q or some subset of those ions. This is illustrated in Fig. 1. In the top panel, the gates on the C^+ and O^+ channels are set wide, while in the bottom case, just the lower KER portion of the ions are selected. These "wide" or "narrow" gate settings are listed in Table I along with the results for each experiment. When the wide gate setting was in place, the C^+ and O^+ ions could originate from a variety or sources. With the narrow gate settings, in contrast, the fitness target involves only uniquely CO^+ dissociation channels, specifically $[C^+ + O]/[C + O^+]$ or $[C + O^+]/[C^+ + O]$.

Somewhat surprisingly, the results indicate that selecting the more specific fitness target does not always improve the ability of the GA to maximize the desirable result. Wide $[C^+/O^+]$ gates, including all of the C^+ and O^+ fragments, produced higher fitness yields than did the more specific $[C^+ + O]/[C + O^+]$ target, which produced a fitness yield only slightly above the level achieved by a transform-limited pulse. On the other hand, when optimizing O^+ yield, the optimal pulse produced a fitness yield of nearly double the transform-limited pulse for $[C + O^+]/[C^+ + O]$ but only about

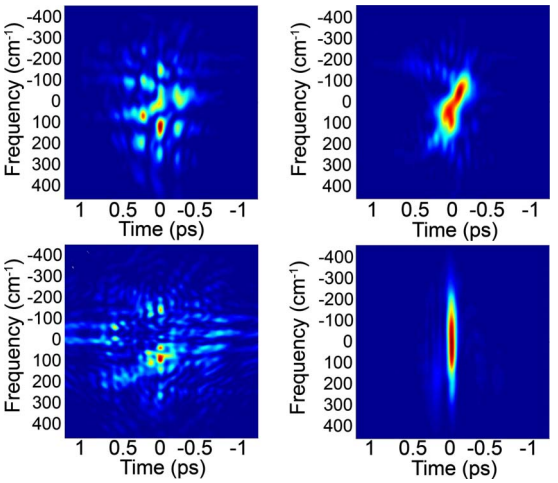

FIG. 2. (Color online) Simulated FROG image for various optimal pulses. (Top left) O^+/C^+ optimization with wide gates and 0.115 mJ/pulse. (Bottom left) narrow gate settings and 0.100 mJ/pulse for the same O^+/C^+ fitness target. (Top right) C^+/O^+ optimization with wide gates and 0.120 mJ/pulse. (Bottom right) C^+/O^+ optimization with narrow gate settings and 0.100 mJ/pulse.

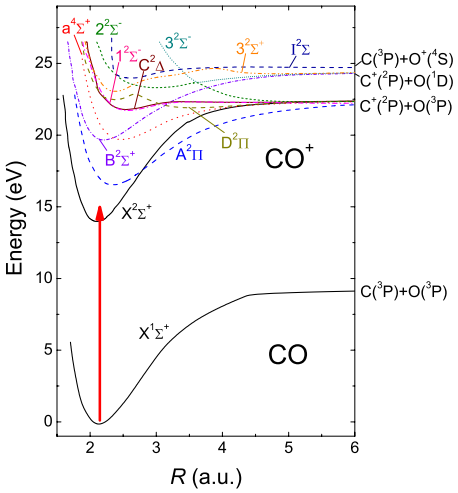

FIG. 3. (Color online) Potential energy curves for CO [45] and various states of CO^+ [46,47]. The red arrow schematically represents the ionization step.

a 20%–25% gain over the transform-limited value with wide $[O^+/C^+]$ gates.

To better understand these results, we examine the characteristics of the optimal pulses. Using the measured bandwidth of the pulse before and after the DAZZLER and the phase values contained in the genes of each pulse, we construct simulated images that mimic the output of a polarization gate frequency-resolved optical gating (FROG) [62]. The optimal pulses for the $[C^+/O^+]$ and $[C^+ + O]/[C + O^+]$ experiments are shown on the right panels of Fig. 2. In this comparison, it appears that the more specific fitness target results in a nearly transform-limited optimal pulse and thus makes it clear why the optimal pulse fitness did not exceed the transform-limited value.

The $[O^+/C^+]$ and $[C+O^+]/[C^+ + O]$ optimization results are more interesting. In this case, the GA must find a compromise between two competing trends. First, previous observations have shown that longer pulses tend to produce more fragmentation [12]. On the other hand, as shown in Fig. 3, the $[C+O^+]$ states have a higher potential energy than the $[C^+ + O]$ states at the separate atom limit [46,47], and this trend continues for asymmetric dissociation from higher charge states. Thus, lower intensity should favor C^+ production. When examining the differences in the TOF spectra obtained using the optimized and transform-limited pulse, it is apparent that the best pulse slightly increases the O^+ yield in some of the higher KER peaks while keeping the same peaks in the C^+ channels nearly constant. The pulse, shown in the top left panel of Fig. 2, is more complex than the pulses obtained in the $[C^+/O^+]$ experiments but still seems to retain a fair amount of intensity.

In contrast, when the gates are narrowed so only the low KER fragments are included, effectively selecting the more specific $[C+O^+]/[C^+ + O]$ fitness target, the TOF spectrum (shown in the bottom panel of Fig. 1) shows that the best pulse retains the yield in the central low KER O^+ peak while reducing the yield in the corresponding region of the C^+ fragments. Examination of the pulse characteristics in the bottom left panel of Fig. 2 shows that the pulse is lengthened compared to the pulse obtained with wide gates and seems to have gained complexity. When considered from the point of view of a simple argument based upon intensity, this is a surprising result. The optimal pulse appears to have found a method that continues to populate the higher lying $[C+O^+]$ states while suppressing the lower lying $[C^+ + O]$ states. With the narrow gates, the optimal fitness was nearly double the transform-limited result, while the wide gate settings resulted in only a 20%–25% gain.

Our results seem to be mixed. In one case, the more specific fitness target resulted in increased control, but in the other it did not. Visual inspection of the optimal pulse shapes would suggest that the narrow gates decreased the pulse complexity (Fig. 2) but the opposite result was true when the inverse ratio was the fitness target. Visual inspection, however, may not be the best measure of complexity in this situation, as some of the optimal pulse may be superfluous. In addition, when the TOF data is examined in conjunction with the potential energy curves shown in Fig. 3, some additional information about possible mechanisms may be extracted. In the next subsections, we examine the pulse shapes and the ion signal information in more detail.

A. Pulse shape analysis

As described previously [9,63], principal control analysis (PCA) [64] may be applied to closed-loop control in an attempt to determine how much of the complex pulse shape is important. The first step in PCA is the construction of the covariance matrix of the set of pulse shapes in the search

$$C_{ij} = \langle \delta_i \delta_j \rangle - \langle \delta_i \rangle \langle \delta_j \rangle, \tag{1}$$

where $\delta_i = x_{i+1} - x_i$, $i = 1, \ldots, n-1$ are the nearest neighbor phase differences, x_i is the ith gene value, and n is the number of genes in each individual. The averaging is performed

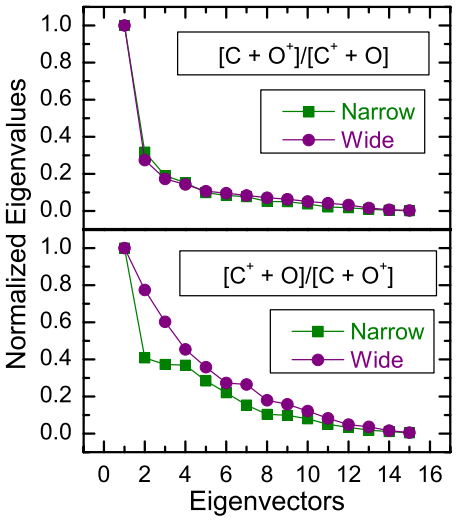

FIG. 4. (Color online) Eigenvalues of the covariance matrices in descending order for the O^+/C^+ (top) and C^+/O^+ (bottom) optimizations.

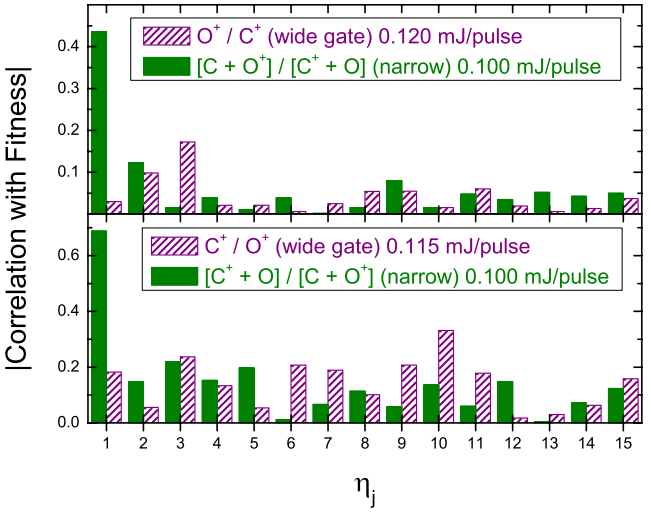

FIG. 5. (Color online) Absolute value of the correlation with fitness as a function of PCA eigenvector, η_j. (Top) comparison of O^+/C^+ optimizations with different gate settings. (Bottom) comparison of the C^+/O^+ optimizations with different gate settings. In both cases, the wide settings produce more principal control directions that correlate with the fitness. The eigenvalues are ordered as in Fig. 4.

over all individuals in the population. After the covariance matrix is constructed, its eigenvectors, η_j, and eigenvalues, λ_j, are calculated. The eigenvalues are a measure of how far the algorithm moved along that eigenvector during its search. The PCA method assumes that the principal control directions (PCDs) are those control directions having the largest eigenvalues. When expressed in the eigenvector basis, the control directions are uncorrelated, and each eigenvector is an independent control direction. The eigenvectors obtained for several of the present measurements are shown in Fig. 4. In each case, many of the 15 eigenvectors seem to have relatively small eigenvalues. Interestingly, the apparently complex pulse shapes produced in attempts to enhance the O^+ yield and reduce the C^+ yield (shown on the left side of Fig. 2) seem to have fewer large eigenvalues than the pulse shapes designed to optimize the opposite ratio.

A further measure of the importance of each eigenvector [9] may be found by calculating the correlation of the projections of the pulse shapes onto the eigenvectors, η_i, with the pulse shape fitness, f,

$$B_{\eta_i} = (\langle \eta_i f \rangle - \langle \eta_i \rangle \langle f \rangle)/\sigma_{\eta_i}\sigma_f, \tag{2}$$

where σ_{η_i} and σ_f represent the standard deviations of their respective subscripts. The best GA solutions for each measurement can then be projected onto the $k<n$ PCDs, u_k, thus reducing the dimension of the control space and producing the essential pulse, $\Sigma_{j=1}^{k} \eta_j u_j(\omega)$.

The results of the correlation with fitness are shown in Fig. 5. Excluding the primary eigenvector which PCA assumes should be the most important control direction, the wide gates produce a larger number of eigenvectors that correlate with fitness. The implication is that it takes a larger number of control directions to parameterize the optimal pulse when a more general fitness target is employed. The effect is not large: the average correlation with fitness for the remaining 14 eigenvectors in the C^+/O^+ cases is 0.11 with narrow gates and 0.14 with wide gates. For the O^+/C^+ experiments, the corresponding numbers are 0.040 with narrow gates and 0.044 with wide gates.

The trend, however, is consistent. The same measurements conducted at lower pulse energy give similar results. Extending to a different channel, we examined the optimization of $[CO^{2+}]/[C^+ + O^+]$ with the laser polarization parallel to the TOF axis of the spectrometer [65]. In this configuration, we set our gates on C^+ fragments initially directed toward the detector and O^+ fragments initially moving away from the detector. The fitness gain was similar to the wide gate settings, which collected all of the C^+ and O^+ fragments. In all cases, narrow gate settings resulted in pulses that required fewer PCDs to describe their essential character than pulses optimized with wide feedback gates.

Ideally, the essential pulse will contain the necessary traits while minimizing irrelevant features. The extent to which this is true in a mathematical sense can be calculated with the preservation formula $P_j = \Sigma_{j=1}^{k} \eta_j^2(\omega)$. These essential pulses may then be programmed into the DAZZLER and the fitness (f) of these pulses verified experimentally. Figure 6 shows the results of this analysis for the $[C+O^+]/[C^+ + O]$ optimization target (the corresponding optimal pulse is shown on the bottom left of Fig. 2). Even with only one principal control direction, in this example, about 90% of both the pulse characteristics and the pulse's ability to control the fragmentation are retained. This result might cause one to wonder about the usefulness of PCA. If the pulse preservation and pulse fitness essentially track each other, it would indicate that there are few superfluous characteristics for PCA to eliminate. Is this a general trend?

Figure 7 demonstrates the relationship between pulse preservation and fitness for all four measurements shown in Fig. 2. This analysis shows that at least in the case of the $[C^+ + O]/[C + O^+]$ experiment in the top panel, the pulse fit-

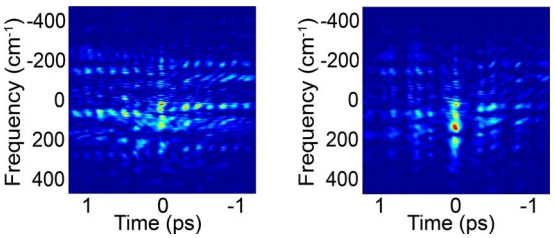

FIG. 6. (Color online) FROG reconstruction of essential pulses for the $[C+O^+]/[C^+ + O]$ target for one PCD (left) and five PCD (right). The FROG plot with all PCD is shown in the bottom left panel of Fig. 2. The mathematical preservation of the 1 PCD reconstruction is 0.90 and 0.93 for the five PCD reconstruction. The corresponding measured relative fitness values are 0.90 and 0.96, as described in the text and shown in Fig. 7.

ness can be considerably higher than the pulse preservation. Furthermore, it seems that a single control direction is enough to retain over 90% of the fitness in each case. Thus, PCA seems effective at eliminating extra features from a pulse while allowing the pulse to still be reasonably effective. The degree of extra features in the pulse, however, seems rather variable. Most of our pulses could be expressed with only a few control directions.

To briefly summarize the key information obtained from the pulse shape analysis: (1) more specific feedback gates seem to result in a statistical reduction in the pulse complexity. In all cases, this was a small effect. Even with the more specific target, the GA may need to identify a pulse that can compensate for intensity variations over the focal volume of the target, and thus some complexity is unavoidable. The combination of more specific target and a limited reduction in pulse complexity may, however, lead to more straightforward investigations of the control mechanism in some cases. (2) Principal control analysis is able to produce pulses with a reduced number of control directions that achieve fitness levels comparable to the fitness using all the control directions. The amount of "extra" characteristics in the optimal pulses varies from measurement to measurement, but we did not observe any "essential" pulse that produced an experimental fitness that was significantly less than the extent to which the pulse characteristics had been preserved.

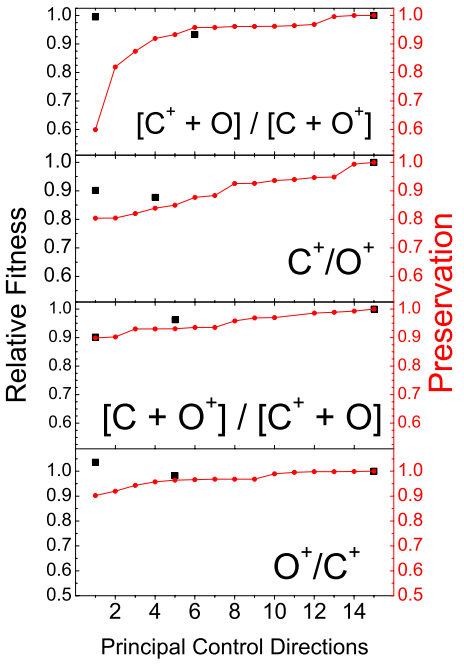

FIG. 7. (Color online) Comparison of the mathematical preservation of pulse characteristics, P_j, (red circles) and the measured fitness for essential pulses (black squares) listed as a function of the number of principal control directions included in the essential pulse. The four measurements shown correspond to the four measurements shown in Fig. 2. The fitness values are normalized to the measured value obtained with the complete pulse (equivalent to 15 PCDs). Values of more than 1.0 most likely indicate scatter in the data rather than a significant enhancement of the fitness value.

B. Ion signal analysis

In addition to simple identification of the ions produced by the laser pulses, the TOF measurement yields some information about the dynamics of the fragmentation. For our spectrometer, the KER from multielectron dissociative ionization can be determined from the potential on the extraction plate of the spectrometer, V_2, the potential on the acceleration plate, V_1, the distance between the plates, d, the mass, m, the charge of the ions, q, and the time difference (Δt) between the forward and backward traveling ions [66]. The complete formula is

$$E_k = \frac{(V_2 - V_1)^2}{8md^2} q^2 \Delta t^2. \tag{3}$$

The time-of-flight spectra, shown in Fig. 1, have several peaks for each ion species. It is interesting to note that the peak locations (and hence the peaks of the KER distributions) remain approximately constant irrespective of whether the molecules are irradiated by a transform-limited or shaped laser pulse. The relative area of the various peaks does change, so by understanding the origin of the different peaks we might be able to determine something about the mechanistic changes caused by the different pulse shapes.

One way to model the KER from these processes is Coulomb explosion (see, for example, Refs. [28,55,67]), in which

$$E_k = \frac{pq}{R_0}, \tag{4}$$

where R_0 is the equilibrium internuclear separation and p and q are the charge states of the carbon and oxygen atoms, respectively. A number of experiments involving diatomic molecules in approximately similar laser fields (e.g., Refs. [68,69]) have found KER values that are lower than ionization at R_0 would predict. A more likely process is multielectron dissociative ionization, which is frequently modeled with a field ionization Coulomb explosion picture [55,69–71]. In this picture, CO^+ is produced on the rising edge of the laser pulse [72,73], and the molecular ion stretches as the field increases. Ionization to CO^{2+} (or higher charge states) is enhanced at some critical internuclear dis-

TABLE II. Comparison of peak values of the KER distributions from the time-of-flight measurements and the expected KER values given by the Coulomb explosion model at R_0 (Eq. (4)) and R_c (Eq. (5)) (see text). The KER values are listed in eV. In Eq. (5), R_c =7.9 atomic units.

Fragment	Channel (p,q)	R_0	R_c	Experiment
C^+	(1,1)	7.30	3.30	4.2
	(1,2)	14.6	5.27	7.5
C^{2+}	(2,2)	29.2	9.20	14.5
O^+	(1,1)	5.48	2.47	3.3
	(2,1)	11.0	3.95	7.0
O^{2+}	(2,2)	21.9	6.90	10.7

tance, R_c. For diatomic molecules with an odd number of electrons, $R_c=4.07/I_p$ [74,75], where I_p is the ionization potential. The KER can then be approximated by the charge state and the separation of the nuclei at the time of ionization [52,55],

$$E_k(p,q) = \frac{1}{4}\left(\frac{1}{R_0} - \frac{1}{R_c}\right) + \frac{pq}{R_c}. \tag{5}$$

Using Eq. (3) and conservation of momentum, we can compare the experimental results with the models described by Eqs. (4) and (5). The comparison is illustrated in Table II.

Our experimental results uniformly fall between the predictions of the two models. Examination of Fig. 1 shows that the peaks are relatively broad, and this suggests that the most likely explanation for the results shown in Table II is that the experiment lacks the resolution to clearly distinguish between dissociation channels from the same CO^{q+}. The results can also indicate, however, that the pulse shapes are producing more complex behavior than is described by either model.

Thus far, the ion signal analysis has ignored the dissociation channels (C^++O or C+O^+) targeted for enhancement with narrow feedback gates. The models discussed above are for multiple ionization rather than dissociative single ionization. We can, however, determine the KER distribution for these events in which only one fragment is charged. This technique, as derived by Schäfer *et al.* [76], uses the shape of the time-of-flight spectrum to derive the KER,

$$P[E_k(t)] = \frac{2m}{(qE)^2}\frac{df(t)}{dt}, \tag{6}$$

where E is the electric field in the extraction region, and $f(t)$ is the number of fragments as a function of their time of flight, t. The E_k distribution for O^+ fragments, which because of their low energy originate predominately from the [C +O^+] channel, is shown in Fig. 8. Both the E_k distribution obtained with the transform-limited pulse and the pulse optimized with the [C+O^+]/[C^++O] target show a similar peak at very low energy. This peak, with a FWHM of around 50 meV, is only slightly above the room temperature thermal distribution. The rest of the distribution, however, is clearly

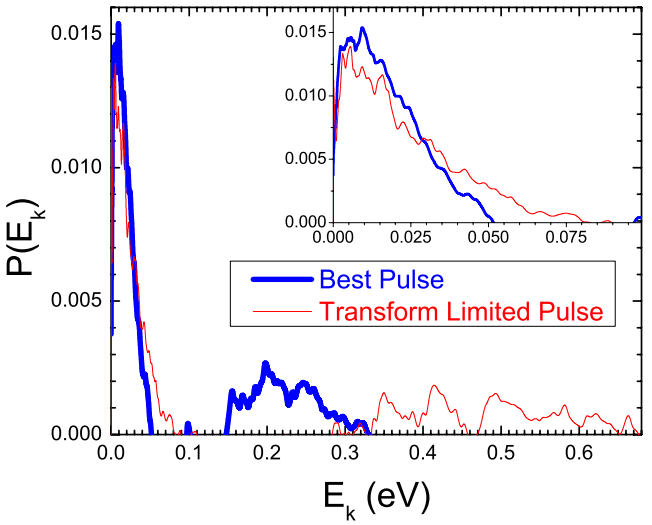

FIG. 8. (Color online) The E_k distributions for O^+ fragments produced by a transform-limited pulse (thin red line) and the pulse optimized to enhance [C+O^+]/[C^++O] (thick blue line). The optimal pulse is shown in the bottom left panel of Fig. 2. This low-energy portion of the E_k spectrum shows the dissociation from the CO^+ ion. The inset shows a magnification of the low-energy peak.

different. The transform-limited pulse produces a wider E_k distribution at somewhat higher energies than the E_k distribution from the optimized pulse.

The potential-energy curves (see Fig. 3) are of some use in trying to understand this information. The available literature shows that the lowest energy curve of CO^+ dissociating into C+O^+ is the I $^2\Sigma$ state [47], which dissociates into C(^{3}P)+O^+(^{4}S) at the separate atom limit. This curve is very strongly repulsive, even at internuclear distances (R) of greater than 2 a.u. It also has a shallow minimum near R =2.5 a.u. and then is very nearly flat at larger R. Given the steepness of the curve at small R, it seems unlikely that a direct ionization mechanism [77,78] would produce the narrow, near zero-energy dissociations observed in Figs. 1 and 8. On the contrary, a reflection of the initial nuclear wavepacket onto the CO^+ I $^2\Sigma$ state after a nearly vertical transition should produce a very wide KER distribution. An electron rescattering mechanism [79] in which the returning electron excites an electron from a lower lying CO^+ state to the C+O^+ final state is also unlikely for the same reasons. The $\sim$2/3 of a laser cycle delay, where the mechanism peaks, allows very little time for the CO^+ to stretch, and therefore the excitation would still land on a steep region of the CO^+ I $^2\Sigma$ curve and result in relatively high KER.

How then does one reach a curve that dissociates to the C+O^+ limit and falls apart very slowly? The answer would seem to be some sort of multiple-step process, as illustrated in Fig. 9. One possibility is that a direct ionization to a C^+ +O curve is followed by, after stretching to a larger R, a subsequent excitation to either the CO^+ I $^2\Sigma$ curve or a curve that crosses that state as illustrated in Fig. 9(a). These sort of events probably would have a KER greater than zero, but it is not unreasonable to suppose that they might make up the higher energy portion of the KER distribution shown in Fig. 8.

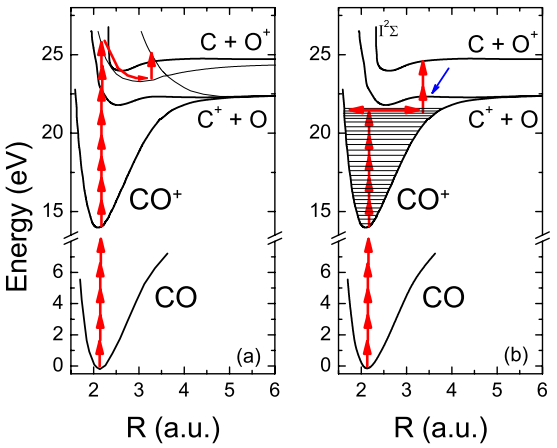

FIG. 9. (Color online) Schematic diagrams illustrating possible ionization mechanisms leading to $[C+O^+]$. (a) A multistep process in which a direct ionization to an excited electronic C^++O state is followed by propagation of the wavepacket to larger R and then excitation to the $C+O^+$ final state. (b) Initial ionization to a highly excited rovibrational state of CO^+ followed by excitation to the $C+O^+$ final state at large R. Given the length of our pulses, it is possible that the CO^+ might oscillate more than once prior to the excitation. An alternative path, noted by the thin blue arrow, would have the excitation to the $C+O^+$ final state occurring during the dissociation of a metastable CO^+ state.

To dissociate with near zero energy, the CO^+ $I\,^2\Sigma$ state would have to be populated at large R. Essentially, just before the outermost electron must decide which atomic center to stay with, it would gain enough energy to reach the higher $C+O^+$ state. In turn, this indicates that the CO^+ must stretch some distance, suggesting that the CO^+ is in a high lying vibrational state prior to the excitation to the $C+O^+$ final state, as illustrated in Fig. 9(b). Another possible route would be from the dissociating metastable CO^+ state, as indicted by the thin blue arrow in Fig. 9(b).

The idea that rovibrational excitation can lead to dissociation has been around for some time. Chelkowski and colleagues speculated that a negatively chirped pulse could take advantage of the molecular anharmonicity, thereby leading to dissociation [80]. The chirp direction on our pulses, however, seems to be predominantly positive and hence in the wrong direction for this explanation. There have been more recent calculations showing that manipulation of the rovibrational excitation of CO is possible with shaped laser pulses [32,81], and the suggested pulses are typically about 1 ps long, albeit at somewhat different frequencies than we are using. Reproducing the general character of these pulses in the time domain is within the capabilities of our laser system. Combined with the KER analysis, it seems reasonable to assume that the $C+O^+$ channel is being populated from excited rovibrational states at large R.

C. Possible control mechanisms

In Secs. III A and III B, we have presented a number of facts about the laser pulse shapes that selectively fragment carbon monoxide. This analysis does not produce incontrovertible evidence pointing to a particular control mechanism in any of the cases we have examined. In this subsection, we will indulge the temptation to speculate about possible control mechanisms based upon this circumstantial evidence. We will consider the four cases shown in Fig. 2.

$\mathbf{O^+/C^+}$ (top left of Fig. 2): this target is the most complicated and produces a complex pulse. Since states that produce O^+ are nearly always higher in energy than states that produce C^+, direct ionization will tend to favor the lower lying states that lead to C^+. Even if there is enough intensity to reach the O^+ states with a transform-limited pulse, when the signal from the entire focal volume is considered, it is difficult to see how the O^+ yield could exceed the C^+ yield. The obvious alternative is to lengthen the pulse to encourage indirect mechanisms. Too long of a pulse, however, will tend to decrease the intensity as well, also favoring C^+ production. Maintaining some intensity is key, since the feedback includes both multiple ionization states.

At ~50 fs, the transform-limited pulses in this experiment are already long enough to stimulate indirect ionization processes [56]. It is possible, however, that the time structure in the optimal O^+/C^+ pulses further increases the indirect ionization pathways. Examination of a plot of intensity vs. time for this pulse shows regular maxima following the central peak at intervals of approximately 100 fs. This duration could match the round trip time for a wavepacket in a highly excited vibrational state of the CO^+.

$\mathbf{[C+O^+]/[C^++O]}$ (bottom left of Fig. 2): the localization of the feedback gate on a specific channel allows the GA to ignore what is happening in the multiple ionization channels, and we note from Fig. 1 that the increase in fitness is caused by a drop in the C^+ yield while the O^+ dissociation channel maintains the level obtained with a transform-limited pulse. As discussed above, the KER information suggests that the final step to the dissociative state happens after the molecular ion has stretched significantly in the field. In the time domain, the optimal pulse contains many smaller subpulses. The spacing is not particularly regular, although it appears much more regular when only one PCD direction is included, as shown on the left side of Fig. 6. The combination of the time structure over a long duration and the very low KER observed in Fig. 8 makes it plausible that this pulse is depleting population from states leading to C^++O and shifting the population to the $C+O^+$ final state. It is likely that this occurs at large R.

$\mathbf{C^+/O^+}$ (top right of Fig. 2): the pulses that optimize the C^+ yield are somewhat easier to understand. As mentioned previously, direct ionization pathways will generally tend to favor C^+. Furthermore, longer pulses tend to produce more fragmentation [12]. The algorithm therefore settles on a fairly intense pulse with some chirp, increasing both the yield of C^+ and the ratio of C^+/O^+.

$\mathbf{[C^++O]/[C+O^+]}$ (bottom right of Fig. 2): with the condition that only the single ionization channel is included, the longer pulses tend to enhance the O^+ yield via the mechanism described above. So the algorithm simply can decide to eliminate the chirp and finds that a nearly transform-limited pulse is the best solution.

It is worth noting that in the four cases above, our speculation about the control mechanisms seems to be better sup-

ported for the narrow gate settings which limit the number of possible final states. It is also worth recalling that this increase in clarity regarding the fragmentation mechanisms does not always come with a corresponding increase in the amount of control. We are, in effect, restricting the information available to the algorithm. Nevertheless, in seeking to better understand this method of coherent control, it is an interesting comparison to examine.

IV. SUMMARY AND OUTLOOK

Using carbon monoxide as a testing ground, we have examined how the specificity of the feedback signal influences the outcome of closed-loop control experiments. Selecting a more specific fitness target did not uniformly improve the level of control in these measurements. Using PCA, however, we observe a small but consistent tendency toward fewer principal control directions being needed to describe the essential characteristics of the pulse that optimized the more specific fitness functions. In short, more specific targets result in slightly simpler optimal pulse shapes. In addition, we verified that the essential pulses constructed using the PCA method replicated the majority of the control obtained with the complete optimal pulses.

Analysis of the high-resolution time-of-flight data for hints about the dissociative ionization mechanisms was inconclusive for the fragments originating from higher charge states of CO^{q+}. The location of the peak of the KER distributions suggested that the final ionization step happened at some point between R_0 and R_c or that our data contained a mix of several processes that we were unable to fully resolve. For the feedback focused on the dissociation of CO^+, however, the KER data was more revealing, indicating that the O^+ final states had small KER values. This leads us to believe that these states were populated by an indirect ionization mechanism at large R. The tendency of the pulses tailored to enhance O^+ yield to be longer in duration than the pulses designed to produce more C^+ is consistent with this idea. While not conclusive, the combination of pulse shape analysis and TOF+KER data allowed us to come up with plausible explanations about the mechanisms behind the optimal pulse shapes.

In fact, because CO is a relatively simple target system, it may even be possible to carry out a more rigorous theoretical treatment of the interaction between the shaped pulse and the molecule. On the experimental side, there are several methods that could be used to make the feedback more specific and/or probe the optimal control mechanisms that have been identified using TOF. An imaging technique [82], such as velocity map imaging (VMI) [83,84], could provide both angular information about the dissociating fragments and higher resolution KER information, especially for the more energetic ions. Furthermore, VMI is fast enough to incorporate directly into the feedback loop. A drawback to both TOF and VMI feedback is that they are uncorrelated. While using an event mode momentum imaging system [85,86] in the feedback loop itself would probably be too slow, it might be possible to correlate TOF signals (e.g., $[C^+ + O^+]$ from CO^{2+}) and then use the momentum imaging to examine the optimal pulses. It will be interesting to see if the incorporation of even more specific targets into feedback loops, whether by using coincidences in the time-of-flight measurement or incorporating additional momentum components from the dissociating ions into the feedback signal, will continue the trends reported here.

The difficulties in understanding the mechanisms underlying these closed-loop control methods have been documented previously [9]. In this article, we report some small steps toward obtaining a more complete understanding of how control is achieved in a diatomic system. While future steps may continue to be challenging, our results suggest the barriers to deconstructing the optimal pulse shapes to reveal the control mechanisms may not be intractable.

ACKNOWLEDGMENTS

The authors gratefully acknowledge Professor Zenghu Chang and his group members for providing laser expertise, Professor Brett DePaola for numerous helpful discussions about working with the DAZZLER, and Siddique Kahn for his assistance constructing the apparatus. This work was supported by National Science Foundation Award No. PHY-0653598 and by the Chemical Sciences, Geosciences, and Biosciences Division, Office of Basic Energy Sciences, Office of Science, U.S. Department of Energy. N.L.S. and E.W. acknowledge additional support provided by the National Science Foundation–Undergraduate Research Center Program No. CHE-0532242 ["The Northern Plains Undergraduate Research Collaboration (NPURC)"].

[1] C. Bardeen, V. Yakovlev, K. Wilson, S. Carpenter, P. Weber, and W. Warren, Chem. Phys. Lett. **280**, 151 (1997).
[2] A. Assion, T. Baumert, M. Bergt, T. Brixner, B. Kiefer, V. Seyfried, M. Strehle, and G. Gerber, Science **282**, 919 (1998).
[3] M. Bergt, T. Brixner, B. Kiefer, M. Strehle, and G. Gerber, J. Phys. Chem. A **103**, 10381 (1999).
[4] R. Bartels, S. Backus, E. Zeek, L. Misoguti, G. Vdovin, I. P. Christov, M. M. Murnane, and H. C. Kapteyn, Nature (London) **406**, 164 (2000).
[5] R. J. Levis, G. M. Menkir, and H. Rabitz, Science **292**, 709 (2001).
[6] J. L. Herek, W. Wohleben, R. J. Cogdell, D. Zeidler, and M. Motzkus, Nature (London) **417**, 533 (2002).
[7] R. S. Minns, J. R. R. Verlet, L. J. Watkins, and H. H. Fielding, J. Chem. Phys. **119**, 5842 (2003).
[8] A. Lindinger, C. Lupulescu, M. Plewicki, F. Vetter, A. Merli, S. M. Weber, and L. Wöste, Phys. Rev. Lett. **93**, 033001 (2004).
[9] E. Wells, K. J. Betsch, C. W. S. Conover, Merrick J. DeWitt, D. Pinkham, and R. R. Jones, Phys. Rev. A **72**, 063406 (2005).

[10] T. Laarmann, I. Shchatsinin, A. Stalmashonak, M. Boyle, N. Zhavoronkov, J. Handt, R. Schmidt, C. P. Schulz, and I. V. Hertel, Phys. Rev. Lett. **98**, 058302 (2007).
[11] D. Pinkham, K. E. Mooney, and R. R. Jones, Phys. Rev. A **75**, 013422 (2007).
[12] V. V. Lozovoy, X. Zhu, T. C. Gunaratne, D. A. Harris, J. C. Shane, and M. Dantus, J. Phys. Chem. A **112**, 3789 (2008).
[13] M. Kotur, T. Weinachht, B. J. Pearson, and S. Matsika, J. Chem. Phys. **130**, 134311 (2009).
[14] A. M. Weiner, Rev. Sci. Instrum. **71**, 1929 (2000).
[15] J. X. Tull, M. A. Dugan, and W. S. Warren, Adv. Magn. Opt. Reson. **20**, 1 (1997).
[16] M. A. Dugan, J. X. Tull, and W. S. Warren, J. Opt. Soc. Am. B **14**, 2348 (1997).
[17] R. S. Judson and H. Rabitz, Phys. Rev. Lett. **68**, 1500 (1992).
[18] B. J. Pearson, J. L. White, T. C. Weinacht, and P. H. Bucksbaum, Phys. Rev. A **63**, 063412 (2001).
[19] D. Zeidler, S. Frey, K.-L. Kompa, and M. Motzkus, Phys. Rev. A **64**, 023420 (2001).
[20] E. David Godlberg, *Genetic Algorithms in Search, Optimization, and Machine Learning* (Addison-Wesley, Boston, 1989).
[21] J. Roslund and H. Rabitz, Phys. Rev. A **79**, 053417 (2009).
[22] J. Roslund, M. Roth, and H. Rabitz, Phys. Rev. A **74**, 043414 (2006).
[23] A. Rothman, T. S. Ho, and H. Rabitz, Phys. Rev. A **73**, 053401 (2006).
[24] C. Daniel, J. Full, L. González, C. Lupulescu, J. Manz, A. Merli, Š. Vajda, and L. Wöste, Science **299**, 536 (2003).
[25] D. Cardoza, M. Baertschy, and T. Weinacht, J. Chem. Phys. **123**, 074315 (2005).
[26] R. A. Bartels, M. M. Murnane, H. C. Kapteyn, I. Christov, and H. Rabitz, Phys. Rev. A **70**, 043404 (2004).
[27] C. Trallero, B. J. Pearson, T. Weinacht, K. Gilliard, and S. Matsika, J. Chem. Phys. **128**, 124107 (2008).
[28] G.-Y. Chen, Z. W. Wang, and W. T. Hill III, Phys. Rev. A **79**, 011401(R) (2009).
[29] L. Bonacina, J. Extermann, A. Rondi, V. Boutou, and J.-P. Wolf, Phys. Rev. A **76**, 023408 (2007).
[30] C. Gollub and R. de Vivie-Riedle, New J. Phys. **11**, 013019 (2009).
[31] D. Weidinger and M. Gruebele, Mol. Phys. **105**, 1999 (2007).
[32] M. Tsubouchi and T. Momose, Phys. Rev. A **77**, 052326 (2008).
[33] T. Brixner, B. Kiefer, and G. Gerber, Chem. Phys. **267**, 241 (2001).
[34] M. Bergt, T. Brixner, C. Dietl, B. Kiefer, and G. Gerber, J. Organomet. Chem. **661**, 199 (2002).
[35] T. Brixner, N. H. Damrauer, G. Krampert, P. Niklaus, and G. Gerber, J. Mod. Opt. **50**, 539 (2003).
[36] R. J. Levis and H. A. Rabitz, J. Phys. Chem. A **106**, 6427 (2002).
[37] C. Daniel, J. Full, L. Gonzalez, C. Kaposta, M. Krenz, C. Lupulescu, J. Manz, S. Minemoto, M. Oppel, P. Rosendo-Francisco, Š. Vajda, and L. Wöste, Chem. Phys. **267**, 247 (2001).
[38] D. Cardoza, F. Langhojer, C. Trallero-Herrero, O. L. A. Monti, and T. Weinacht, Phys. Rev. A **70**, 053406 (2004).
[39] F. Langhojer, D. Cardoza, M. Baertschy, and T. Weinacht, J. Chem. Phys. **122**, 014102 (2005).
[40] D. Cardoza, M. Baerschy, and T. Weinacht, Chem. Phys. Lett. **411**, 311 (2005).
[41] D. Cardoza, B. J. Pearson, M. Baertschy, and T. Weinacht, Photochem. Photobiol. Sci. **180**, 277 (2006).
[42] I. Ben-Itzhak, V. Krishnamurthi, K. D. Carnes, H. Aliabadi, H. Knudsen, U. Mikkelsen, and B. D. Esry, J. Phys. B **29**, L21 (1996).
[43] E. Wells, B. D. Esry, K. D. Carnes, and I. Ben-Itzhak, Phys. Rev. A **62**, 062707 (2000).
[44] M. Lundqvist, P. Baltzer, D. Edvardsson, L. Karlsson, and B. Wannberg, Phys. Rev. Lett. **75**, 1058 (1995).
[45] P. H. Krupenie and S. Weissman, J. Chem. Phys. **43**, 1529 (1965).
[46] K. Okada and S. Iwata, J. Chem. Phys. **112**, 1804 (2000).
[47] F. Falk, M. Carlsson-Göthe, B. Wannberg, F. Falk, L. Karlsson, S. Svensson, and P. Baltzer, Phys. Rev. A **44**, R17 (1991).
[48] T. Šedivcová, P. R. Žd'ánská, and V. Špirko, and J. Fišer, J. Chem. Phys. **124**, 214303 (2006).
[49] G. Handke, F. Tarantelli, and L. S. Cederbaum, Phys. Rev. Lett. **76**, 896 (1996).
[50] J. Lavancier, D. Normand, C. Cornaggia, J. Morellec, and H. X. Liu, Phys. Rev. A **43**, 1461 (1991).
[51] C. Cornaggia, J. Lavancier, D. Normand, J. Morellec, P. Agostini, J. P. Chambaret, and A. Antonetti, Phys. Rev. A **44**, 4499 (1991).
[52] H.-Z. Ren, R. Ma, J. Chen, X. Li, H. Yang, and Q. Gong, J. Phys. B **36**, 2179 (2003).
[53] A. S. Alnaser, C. M. Maharjan, X. M. Tong, B. Ulrich, P. Ranitovic, B. Shan, Z. Chang, C. D. Lin, C. L. Cocke, and I. V. Litvinyuk, Phys. Rev. A **71**, 031403(R) (2005).
[54] C. Guo, Phys. Rev. A **73**, 041401(R) (2006).
[55] Q. Liang, C. Wu, Z. Wu, M. Liu, Y. Deng, and Q. Gong, Phys. Rev. A **79**, 045401 (2009).
[56] B. Gaire, J. McKenna, N. G. Johnson, A. M. Sayler, E. Parke, K. D. Carnes, and I. Ben-Itzhak, Phys. Rev. A **79**, 063414 (2009).
[57] F. Verluise, V. Laude, Z. Cheng, Ch. Spielmann, and P. Tournois, Opt. Lett. **25**, 575 (2000).
[58] Fastlite Ultrafast Scientific Instrumentation, Campus de l'Ecole Polytechnique 91128 Palaseau, France (http://fastlite2.siteo.com/en/index.xml).
[59] W. C. Wiley and I. H. McLaren, Rev. Sci. Instrum. **26**, 1150 (1955).
[60] The software for this work used the GAlib genetic algorithm package, written by Matthew Wall at the Massachusetts Institute of Technology. The library is available at http://lancet.mit.edu/ga/.
[61] D. A. Dahl, *SIMION 3D version 7.0* (Idaho National Engineering Laboratory, Idaho Falls, 2000).
[62] R. Trebino, K. W. DeLong, D. N. Fittinghoff, J. N. Sweetser, M. A. Krumbuegel, and D. J. Kane, Rev. Sci. Instrum. **68**, 3277 (1997).
[63] J. L. White, B. J. Pearson, and P. H. Bucksbaum, J. Phys. B **37**, L399 (2004).
[64] I. T. Jolliffe, *Principal Component Analysis*, 2nd ed. (Springer, Berlin, 2002).
[65] E. Wells, J. McKenna, A. M. Sayler, B. Jochim, N. Gregerson, R. Averin, M. Zohrabi, K. D. Carnes, and I. Ben-Itzhak, J. Phys. B (to be published).
[66] I. Ben-Itzhak, S. G. Ginther, and K. D. Carnes, Nucl. Instrum. Methods Phys. Res. B **66**, 401 (1992).

[67] S. Shimizu, J. Kou, S. Kawato, K. Shimizu, S. Sakabe, and N. Nakashima, Chem. Phys. Lett. **317**, 609 (2000).
[68] C. Ellert and P. B. Corkum, Phys. Rev. A **59**, R3170 (1999).
[69] J. McKenna *et al.*, Phys. Rev. A **73**, 043401 (2006).
[70] J. H. Posthumus, A. J. Giles, M. R. Thompson, W. Shaikh, A. J. Langley, L. J. Franinski, and K. Codling, J. Phys. B **29**, L525 (1996).
[71] J. H. Posthumus, A. J. Giles, M. R. Thompson, and K. Codling, J. Phys. B **29**, 5811 (1996).
[72] X. Urbain, B. Fabre, V. M. Andrianarijaona, J. Jureta, J. H. Posthumus, A. Saenz, E. Baldit, and C. Cornaggia, Phys. Rev. Lett. **92**, 163004 (2004).
[73] A. Requate, A. Becker, and F. H. M. Faisal, Phys. Rev. A **73**, 033406 (2006).
[74] S. Chelkowski and A. D. Bandrauk, J. Phys. B **28**, L723 (1995).
[75] A. D. Bandrauk and H. Z. Lu, Phys. Rev. A **62**, 053406 (2000).
[76] K. Schäfer, W. Y. Baek, K. Förster, D. Gassen and W. Neuwrith, Z. Phys. D: At., Mol. Clusters **21**, 137 (1991).
[77] F. Legare, I. V. Litvinyuk, P. W. Dooley, F. Quere, A. D. Bandrauk, D. M. Villeneuve, and P. B. Corkum, Phys. Rev. Lett. **91**, 093002 (2003).
[78] A. S. Alnaser, X. M. Tong, T. Osipov, S. Voss, C. M. Maharjan, P. Ranitovic, B. Ulrich, B. Shan, Z. Chang, C. D. Lin, and C. L. Cocke, Phys. Rev. Lett. **93**, 183202 (2004).
[79] P. B. Corkum, Phys. Rev. Lett. **71**, 1994 (1993).
[80] S. Chelkowski, A. D. Bandrauk, and P. B. Corkum, Phys. Rev. Lett. **65**, 2355 (1990).
[81] T. Herrmann, Q. Ren, G. G. Balint-Kurti, and F. R. Manby, J. Chem. Phys. **126**, 224309 (2007).
[82] B. J. Whitaker, *Imaging in Molecular Dynamics: Technology and Applications (A User's Guide)* (Cambridge University Press, Cambridge, 2003).
[83] A. T. J. B. Eppink and D. H. Parker, Rev. Sci. Instrum. **68**, 3477 (1997).
[84] O. Ghafur, W. Siu, P. Johnsson, M. F. Kling, M. Drescher, and M. J. J. Vrakking, Rev. Sci. Instrum. **80**, 033110 (2009).
[85] R. Dörner *et al.*, Phys. Rep. **330**, 95 (2000).
[86] J. Ullrich, R. Moshammer, A. Dorn, R. Dörner, L. Ph. H. Schmidt, and H. Schmidt-Böcking, Rep. Prog. Phys. **66**, 1463 (2003).